Northumbria Research Link

www.northumbria.ac.uk/nrl

northumbria
UNIVERSITY NEWCASTLE

PbSe quantum dots-based chemiresistors for room-temperature NO$_2$ detection

Min Li[a, b]

Jingting Luo[a, *]
luojt@szu.edu.cn

Chen Fu[a]

Hao Kan[c]

Zhen Huang[c]

Wangman Huang[c]

Shuqin Yang[c]

Jianbing Zhang[c]

Jiang Tang[d]

Yongqing Fu[e]

Honglang Li[f]

Huan Liu[c, *]
huan@mail.hust.edu.cn

[a]Shenzhen Key Laboratory of Advanced Thin Films and Applications, College of Physics and Energy, Shenzhen University, 518060, Shenzhen, China

[b]Key Laboratory of Optoelectronic Devices and Systems of Ministry of Education and Guangdong Province, College of Optoelectronic Engineering, Shenzhen University, Shenzhen, 518060, China

[c]School of Optical and Electronic Information, Huazhong University of Sciences and Technology, 1037 Luoyu Road, Wuhan, Hubei, 430074, China

[d]Wuhan National Laboratory for Optoelectronics, Huazhong University of Sciences and Technology, 1037 Luoyu Road, Wuhan, Hubei, 430074, China

[e]Faculty of Engineering and Environment, Northumbria University, Newcastle upon Tyne, NE1 8ST, UK

[f]Institute of Acoustics, Chinese Academy of Sciences, 100190, Beijing, China

*Corresponding authors.

Abstract

Colloidal quantum dots (CQDs) are promising building blocks for low-cost and high-performance gas sensors due to their excellent solution processability and extremely small size. Among chalcogenide CQDs, PbSe has a large exciton Bohr radius and exhibits strong confinement energies, facilitating the fast charge-carrier transport. However, CQDs-based devices are susceptible to degrade due to the poor stability of CQDs. Here, in order to obtain air-stable PbSe CQDs for gas sensing application, we synthesized PbSe CQDs using a cation exchange method with in situ chloride and cadmium passivation. The sharp absorption peak in UV–vis absorption spectra confirmed strong quantum confinement in the PbSe CQDs and their average diameter was estimated to be 2.87 ± 0.23 nm. To construct gas sensors, PbSe CQDs were spin-coated onto ceramic substrates and then Pb(NO$_3$)$_2$ treatment was carried out to remove the long-chain ligands surrounding PbSe CQDs. At 25 °C, the sensor was highly sensitive and selective to NO$_2$ with a response of 22.3 at 50 ppm and a fast response time of 7 s. Moreover, the sensor response showed a 85.2% stability as the time increased up to 20 days, suggesting the potential applications of PbSe CQDs for NO$_2$ monitoring at room temperature.

1 Introduction

Highly sensitive gas sensors for detecting tiny amounts of toxic and hazardous gases play a vital role in our daily life for public safety, industrial processes, medical diagnosis, and continuous monitoring of environmental pollution [1,2]. To date, worldwide effort has been made to develop reliable gas sensors with high sensitivity and selectivity, and rapid progress has been achieved driven by the emerging nanoscience and nanotechnology [3-5].

Recently, low-dimensional nanostructured materials with tailored structures have expressed great potential for serving as the sensing layer of gas sensors [6-9]. Their performance can be significantly enhanced through reducing the dimension of the gas-sensing materials. Specifically, zero-dimensional nanoparticles were extensively used to make gas sensors because of their unique electrical and optical properties. For example, Pd nanoparticles [10] were used in surface acoustic wave H_2 sensor, ZnO [11] and $BaTiO_3$ [12] nanoparticles were used for detection of formaldehyde and H_2S, respectively. However, one of the major challenges faced in the development of nanoparticle-based gas sensors is the difficulty in obtaining various sizes of nanoparticles below 10 nm as well as the lack of precise control of their size distribution, because smaller particles are expected to have more gas adsorption sites.

Colloidal quantum dots (CQDs), semiconductor nanoparticles synthesized and suspended in the solution phase, display certain merits due to their special structures and properties. First, being highly tunable material, CQDs possess flexible adjustability of sizes, with advantages of extremely small size and narrow size distribution [13]. Second, the grain size of CQDs is comparable with the Debye length, facilitating the fast transfer of the charge and superior gas-sensing properties compared with their bulk counterparts. These are mainly due to the small-size effect in which decreasing crystal size can achieve much larger surface areas which facilitates the gas adsorption [14]. Third, the solution processability of CQDs enabled it to be self-assembled into thin-film quantum dot solids, in which the size and quantum confinement of CQDs can be conserved. These features make devices based on CQDs very promising for the construction of thin film gas sensors. In our previous work, much of the progress in chemiresistive gas sensor was based on lead sulfide (PbS) CQDs because of their well-developed synthesis techniques [15-18]. However, there is currently considerable interest in extending this work to other lead chalcogenide CQDs.

Among the lead chalcogenide family, lead selenide (PbSe) have long been known as versatile functional materials for applications in electronic circuitry [19], field-effect transistors [20], solar cells [21] and photodetectors [22] due to its attractive photoelectric properties. With the small bulk bandgap of 0.28 eV [23] and large exciton Bohr radius of 46 nm [24], which is twice higher than that of PbS (18 nm), PbSe CQDs attain a strong confinement of the electron–hole pair and should induce a significant wave function leakage. Therefore the electronic coupling between adjacent CQDs could be enhanced, facilitating the charge-carrier transport [25]. What's more, the electronic properties of PbSe CQDs that measured macroscopically could sensitively make changes at CQDs surface [26], favoring for high response upon the presence of specific gases. However, PbSe has not been explored as a gas sensing material, although there are literatures using CdSe [27,28], ZnSe [29] and SnSe [30] in gas sensing applications.

In this study, we demonstrated PbSe CQDs-based gas sensors for room temperature NO_2 detection. Noted that CQDs are highly susceptible to oxidation when exposed to ambient air for a long term, making the performance of CQDs-based devices tend to quickly degrade. Thus, to improve the air stability of CQDs, here we synthesized the PbSe CQDs through a cation exchange reaction that converts CdSe CQDs directly into PbSe CQDs with in situ chloride and cadmium passivation. Impressively, gas sensor devices based on PbSe CQDs exhibited high sensitivity, superior selectivity, full reversibility and good long-term stability to low concentration of NO_2 gas.

2 Experimental details

2.1 CQDs synthesis and sensor fabrication

The PbSe CQDs were synthesized via a cation exchange route with some modifications [31]. We first synthesized CdSe CQDs through a hot-injection method as follows: The Cd precursor was made by dispersing 0.512 g CdO in 3.5 mL oleic acid (OA) and 30 mL 1-octodecene (ODE), and then the solution was heated at 260 °C for 20 min. The Se precursor was prepared by dissolving 0.315 g Se powder into 10 mL ODE, then the solution was sonicated for 5 min to form a uniform dispersion. When the solution of Cd precursor was cooled down to 220 °C, the heating mantle was removed, and 5 mL of Se precursor was rapidly injected. After the injection, the solution in the flask was transferred into a cold water bath to be cooled down to room temperature. The product (CdSe CQDs) was rinsed for three times using hexane, chloroform and ethanol, and finally dispersed in 10 mL ODE.

After that, 0.84 g $PbCl_2$ was dissolved in 10 mL oleylamine (OLA) to obtain the Pb precursor. The solution was degassed under vacuum at 80 °C and then heated to 150 °C under nitrogen atmosphere for 30 min. Then, 5 mL of CdSe CQDs dispersed in ODE was swiftly injected into the Pb precursor, which produces black-brown precipitates. The reaction flask was immersed into a cold water bath and allowed to cool down to 80 °C, then 10 mL hexane was added. When the temperature was further cooled to 30 °C, 8 mL OA was added and the solution was stirred for 15 min. Finally, the precipitates were washed for 2–3 times using hexane and ethanol, and then dispersed in octane at a concentration of 50 mg/mL.

Preparation processes for the PbSe CQDs synthesis and film fabrication were schematically shown in Fig. 1. To fabricate gas sensor, alumina ceramic plate with a dimension of 15 × 15 × 0.8 mm was used as the substrate which was pre-patterned with interdigital Ag electrodes. The film was deposited using layer-by-layer spin coating method followed by the ligand exchange treatment as explained below. Briefly, a few drops of PbSe CQDs solution were dropped onto the substrate, which was then spun at 2000 rpm for 15 s. Then the obtained PbSe CQDs film was soaked with $Pb(NO_3)_2$ solution (10 mg/mL in absolute methanol) using a dropper for ligand exchange for 45 s. The $Pb(NO_3)_2$ solution was spun at a speed of 2000 rpm in order to dry the solvent. This soaking-dry treatment was repeated twice. Finally the film was washed by absolute methanol for three times. To make the final sensor devices, the film deposition and ligand exchange treatment processes was repeated again and resulted in two-layered PbSe CQDs films.
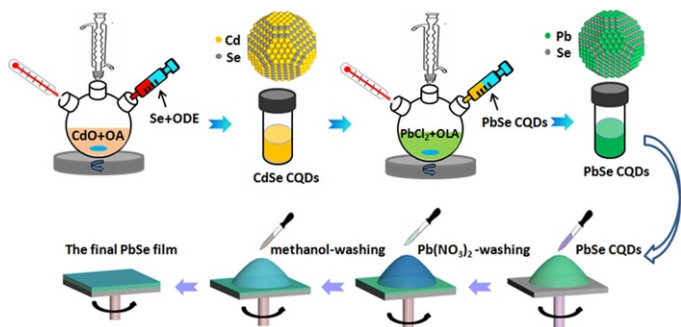

Fig. 1 Schematic diagram illustrating the process from PbSe CQDs synthesis to sensor fabrication.

alt-text: Fig. 1

2.2 Characterization

X-ray diffraction (XRD) measurements were performed using a diffractometer (MAXima_XXRD-7000, Shimadzu, Japan) with Cu K α radiation in the 2-theta range of 10°–80°. High-resolution transmission electron microscopy (HRTEM) images were obtained using JEOL 2100F microscope with an accelerating voltage of 200 kV. UV–vis absorption spectra were obtained using a PerkinElmer Lambda 950 UV/Vis/NIR spectrophotometer. The photoluminescence (PL) spectra were measured with an Edinburgh FLS 980 fluorescence spectrometer at the excitation wavelength of 532 nm. Fourier transform infrared (FTIR) spectroscopy analysis of the CQDs films deposited on quartz glass substrate was conducted with a Bruker Vertex 70 infrared spectrometer. Surface morphologies of the PbSe CQDs films were characterized using a scanning electron microscope (SEM, Zeiss Supra 55). Surface elements and chemical states of the PbSe CQDs films were characterized using X-ray photoelectron spectroscopy (XPS) with an AXIS-ULTRA DLD–600 W system (Kratos, Japan). The electrical properties of the PbSe CQDs film was measured at room temperature by the Hall Effect measurement (ECT, ET-9000). The sample was deposited on a quartz glass substrate of 1 cm × 1 cm size. Four metal circular dots were deposited on four corners of the film for better contact with the probe. Solartron impedance analyzer (Model: 1260) in the frequency range of 1 Hz–1 MHz was used for impedance measurement.

2.3 Measurement of gas sensing properties

Gas-sensing properties of the sensor were evaluated using a CGS-4TPs intelligent gas-sensing analysis system under laboratory conditions (50 ± 10 RH%, 25 ± 1 °C). The sensor was put into the test chamber which was initially filled with fresh air. When the resistance of the sensor was stable, target gas with desired concentrations determined by the volume ratio was injected into the chamber using syringes. The target gas used in the study was mixed by NO_2 and N_2 gases both with the high purity of 99.9% and the volume ratio of NO_2 and N_2 was 1:49. As the sensor resistance reached a constant value, the chamber lid was then opened to allow the sensor resistance to be recovered in the air. The response of the gas sensor is defined as R_a/R_g, where R_a is the resistance of the sensor in air (base resistance) and Rg is the resistance of the sensor in the target gas. The response time was defined as the time taken by the sensor to achieve 90% of the total resistance change in the case of gas adsorption. Similarly, the recovery time was defined as the time taken by the sensor response to reduce to 10% of its maximal value in the case of gas desorption.

3 Results and discussion

3.1 Optical, structural and morphological characteristics

As described in Section 2, we first synthesized the brilliant yellow CdSe CQDs dispersed in ODE, and then it was injected into a hot $PbCl_2$/OLA mixture that promoted direct cation exchange of Cd^{2+} for Pb^{2+} in a single reaction step. Finally, the dark brown PbSe CQDs solution well-dispersed in octane was obtained. The UV–vis absorption spectra of the solutions were shown in Fig. 2. The PbSe CQDs (Fig. 2a) exhibited a clearly shifted band edge absorption peak centered at 950 nm and the corresponding average diameter was estimated to be 2.87 nm, according to the following equation proposed by Zou et al. [32]:

$$d\left(\lambda\right) = \left(\lambda - 143.75\right)/281.25 \qquad\qquad\qquad\qquad \textbf{(1)}$$

where d and λ were the diameter and absorption peak of the CQDs respectively. To further estimate its size distribution, we took 50 data points varying between 860 and 1005 nm from the absorption spectra and calculated the corresponding sizes according to equation 1. Then the corresponding size distribution histogram was plotted in Fig. 2b and fitted using Gaussian function. Based on this estimation, the average value of the particle diameter of PbSe CQDs was 2.87 nm with a standard deviation of 0.23 nm, yielding a relatively narrow size dispersion of 8%. In addition, the PbSe CQDs synthesized in this paper showed a prominently widened band gap of 1.30 eV compared to its bulk band gap (0.28 eV) and thus confirmed the quantum confinement feature of the as-synthesized PbSe CQDs. Fig. 2c showed the absorption spectra of the CdSe CQDs. The maximum intensity peak observed for the sample corresponded to a wavelength of around 465 nm, which could be attributed to the exciton state of $1S_{3/2}$-$1S_e$ [33]. Excitonic absorption due to the exciton state of $2S_{1/2}$-$1S_e$ (375 nm) and $2S_{3/2}$-$1S_e$ (430 nm) were also shown in Fig. 2c. The size of the CdSe CQDs was determined to be about 2.1 nm by using the sizing curve given by Peng et. al [34].
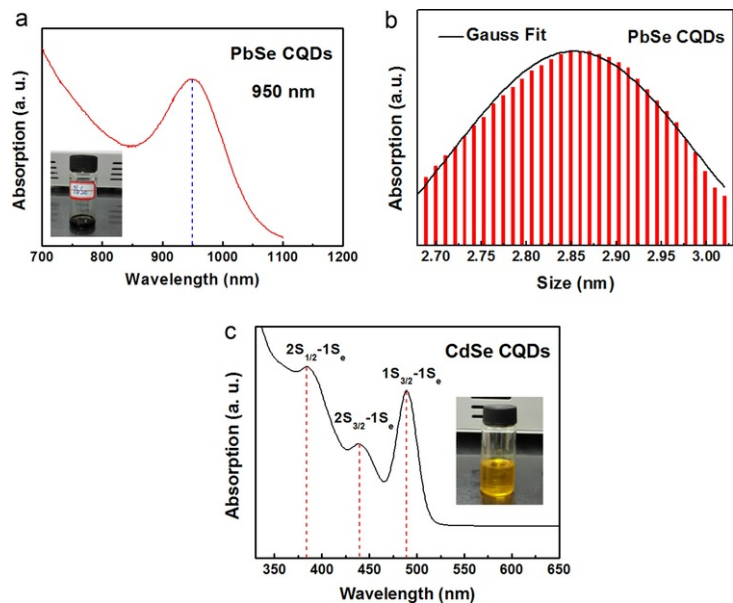

Fig. 2 (a) UV–vis absorption spectra and (b) Histogram of size distribution and fitting of the as-prepared PbSe CQDs, (c) UV–vis absorption spectra of the as-prepared CdSe CQDs.

alt-text: Fig. 2

Fig. 3 showed the XRD pattern of the as-synthesized PbSe CQDs powder. The positions of the diffraction peaks at 2θ = 25.16°, 29.14°, 41.68°, 49.33°, 51.66°, 60.41°, 66.49°, 68.48°, 76.08° can be assigned to the scattering from (111), (200), (220), (311), (222), (400), (331), (420) and (422) planes of the cubic PbSe structure respectively, which were well consistent with the standard card (JCPDS No. 06-0354) of the cubic phase PbSe. The XRD pattern of the starting CdSe CQDs to those of the final PbSe CQDs was also compared and no evidence of residual CdSe was found, indicating that the CdSe CQDs were fully converted to PbSe CQDs during the direct cation exchange reaction.
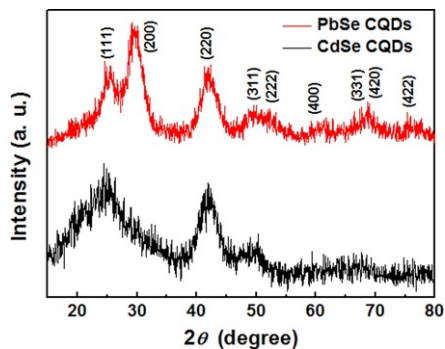
Fig. 3 XRD patterns of the as-prepared PbSe and CdSe CQDs.

alt-text: Fig. 3

HRTEM were employed to further analyze the interior microstructure of the as-synthesized samples. Fig. 4a and b represented the HRTEM images of PbSe and CdSe CQDs, respectively. Nearly spherical and uniformly distributed crystals could be observed. The average particle sizes calculated from the micrograph were found to be 2.8 ± 0.3 nm and 2.2 ± 0.2 nm for the PbSe and CdSe CQDs respectively, which were consistent with the UV–vis results. The well-developed lattice fringes could be clearly observed in Fig. 4c and d, suggestive of the highly-crystallized single crystalline nature of the PbSe and CdSe CQDs. The lattice constants calculated from the lattice fringes in Fig. 4c and the fast Fourier transform (FFT) pattern were 0.35 nm and 0.30 nm, which were corresponding to (111) and (200) crystal planes of lead selenide and in a good agreement with the XRD results.
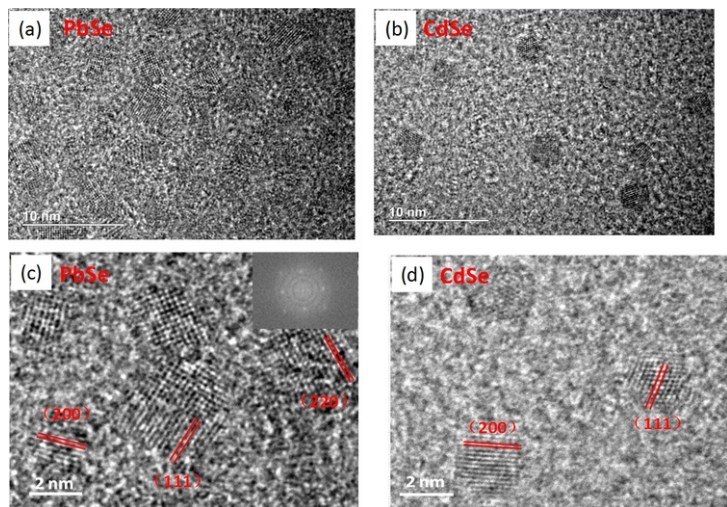

Fig. 4 HRTEM images of the as-prepared (a, c) PbSe CQDs and (b, d) CdSe CQDs. Inset was the corresponding FFT pattern.

alt-text: Fig. 4

3.2 Characterization of PbSe CQDs film

In the synthesis of PbSe CQDs, OA and OLA were used as the surface ligands which could avoid agglomeration of CQDs and enable their solution processability in octane. Therefore, the surface of the as-synthesized PbSe CQDs were capped by abundant OA and OLA ligands, which can be confirmed from the FTIR spectra. The as-prepared PbSe CQDs film (untreated, black line in Fig. 5a) was fabricated on the quartz glass substrate for FTIR analysis. The transmittance peaks at 2850–2920 cm^{-1} characteristic of the aliphatic C

—

H stretching bands could be observed, suggestive of the presence of OA and OLA ligands in the as-synthesized PbSe CQDs. However, these organic ligands with long hydrocarbon chains were generally unwanted in the sensor

fabrication, since they might act as an insulating layer between semiconductors and electrodes and thus hinder both the carrier transfer and gas adsorption [35]. Therefore, in order to remove the OA and OLA ligands capped on the PbSe CQDs surface, we conducted a simple surface ligand exchange treatment in the film deposition process of CQDs, similar to our previous work [15]. In this paper, the short inorganic ligand of $Pb(NO_3)_2$ was employed for exchange of those long-chain ligands. Fig. 5a (red line) demonstrated significant reduction in the C—H stretching peaks at 2854, and 2929 and 2961 cm^{-1} for the $Pb(NO_3)_2$-treated PbSe CQDs film, indicating that most of the OA and OLA ligands were successfully removed by this surface inorganic ion treatment and thus the CQDs film was allowed to be fully exposed to the target gas molecules. Fig. 5b displayed the absorption spectra of the untreated and $Pb(NO_3)_2$-treated PbSe CQDs films. It indicated that the excitonic absorption peak remained after the ligand exchange treatment and its peak position at 950 nm was almost identical to the untreated film. These clearly confirmed that the $Pb(NO_3)_2$ treatment could remove the OA and OLA ligands as well as conserve of the strong quantum confinement and band gap in the prepared PbSe CQDs film.
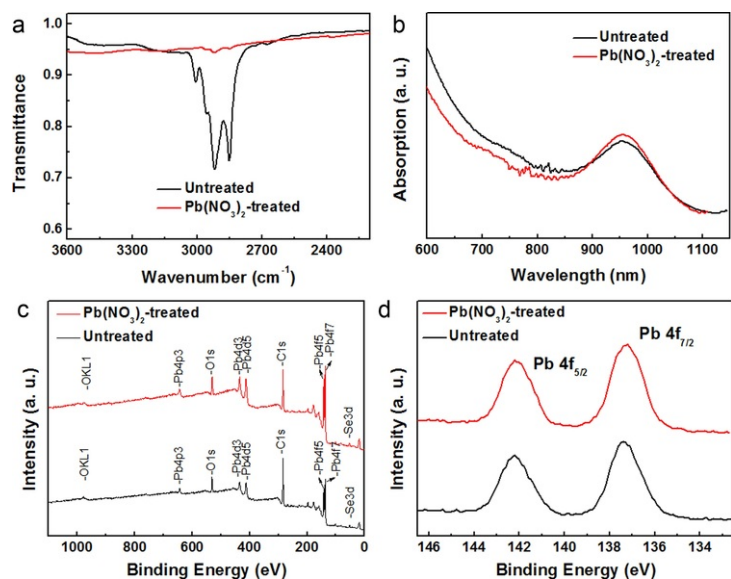

Fig. 5 (a) FTIR spectra, (b) absorption spectra, (c) survey XPS spectra and (d) Pb 4f core-level XPS spectra of the untreated and $Pb(NO_3)_2$-treated PbSe CQDs films.

alt-text: Fig. 5

The surface elements and chemical states of PbSe CQDs film after Pb salt-exchange treatment were examined using XPS analysis. The survey XPS spectra were shown in Fig. 5c, which showed that the main constituent elements of the samples were Pb, Se, C and O. The detected C and O were due to oleate residual and CO_2 contamination [15]. The atomic ratio of Pb to Se was founded to be 1.13 and 1.42 for the untreated and $Pb(NO_3)_2$-treated PbSe films respectively. It revealed that abundant Pb cations binding on the CQDs surfaces were introduced through $Pb(NO_3)_2$ treatment and thus resulted in an increase of the amount of Pb. As shown in Fig. 5d, the Pb 4f core-level spectra for the untreated sample exhibited two well-defined and symmetric peaks centered at 137.4 and 142.2 eV. They were corresponding to Pb $4f_{7/2}$ and $4f_{5/2}$, respectively, consistent with the spectral values for PbSe [36].The characteristic spectral peak attributed to the Pb 4f associated with PbO and Pb_3O_4 centered at around 138.8 eV were not observed in the result, indicating the purity of the prepared PbSe film [37]. There was no obvious shift in the peak position of Pb 4f after $Pb(NO_3)_2$ treatment, suggesting that there was no apparent changes of the chemical environment of Pb with the treatment procedure.

The top-view SEM images shown in Fig. 6 compared the surface morphologies of the PbSe CQDs films before and after the solid-state ligand exchange treatment. There were clearly significant changes in the surface morphologies. The untreated-PbSe film showed the tightly distributed spherical grains on the whole surface. After $Pb(NO_3)_2$ treatment, these grains became separated and some small cracks were observed among them, resulting in porous morphology. This was easily explained by the volume shrinkage induced by the removal of the bulky OA and OLA ligands. The obtained porous morphology would be advantageous for gas sensing applications since porous microstructure is helpful for the gas adsorption and diffusion.
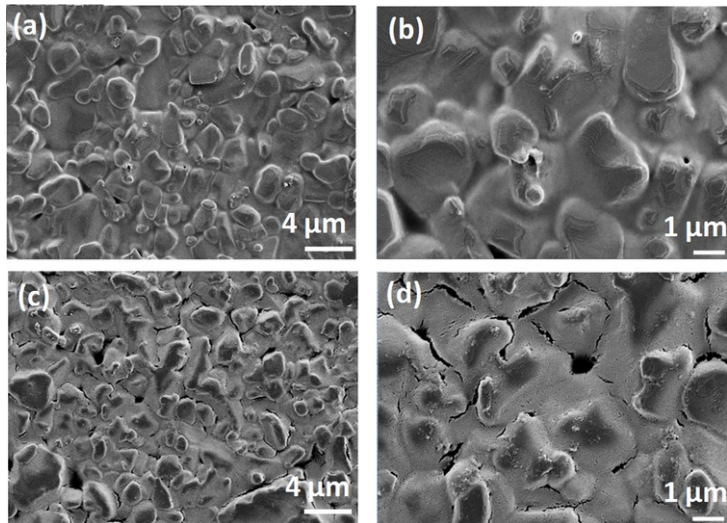
Fig. 6 The film morphology of the (a, b) untreated and (c, d) Pb(NO$_3$)$_2$-treated PbSe CQDs films.

alt-text: Fig. 6

3.3 Gas-sensing properties

Fig. 7a showed the real-time resistance changes of the Pb(NO$_3$)$_2$-treated PbSe CQDs sensor toward 50 ppm NO$_2$ at 25 °C, 50 °C, 75 °C and 90 °C. As the temperature increased, both the base resistance and sensor response decreased. When the temperature exceeded 75 °C, the sensor did not respond to NO$_2$. The response of the sensor to 50 ppm NO$_2$ was the highest at 25 °C and thus, we chose 25 °C as the optimal operation temperature. The repetitive cycles of resistance variation of the sensor toward NO$_2$ with the fixed concentration of 50 ppm at 25 °C were demonstrated in Fig. 7b. Initially, the sensor showed a relatively stable resistance of 38.6 MΩ in air, after the supply of NO$_2$ gas into the test chamber (i.e., the adsorption of gas on the sensor surface), the resistance decreased rapidly and reached a saturated value. After the NO$_2$ gas was stopped followed by the supply of fresh air by opening the chamber lid (desorption), the sensor resistance gradually returned to its original position, indicating the full baseline recovery. The corresponding response curves of the sensor were presented in Fig. 7c. The sensor exhibited a good repeatability after repeated testing cycles, as the sensor showed a nearly constant amplitude of the initial response without any obvious changes after consecutively three tests exposing to the same NO$_2$ concentration. The response of the PbSe CQDs sensor to 50 ppm of NO$_2$ gas was calculated to be 22.3, with the response and recovery times of 7 s and 39 s respectively, which showed an extremely high response and fasted response/recovery speed compared to the other NO$_2$ sensors based on metal sulfide or selenide semiconductors reported in literatures (see Table 1). Therefore, PbSe CQDs can be used as a promising gas sensor material toward oxidizing NO$_2$ gas at room temperature. The small particle size and high surface-to-volume ratio of PbSe CQDs as well as its porous film morphology might guarantee the high sensitivity and fast response speed.
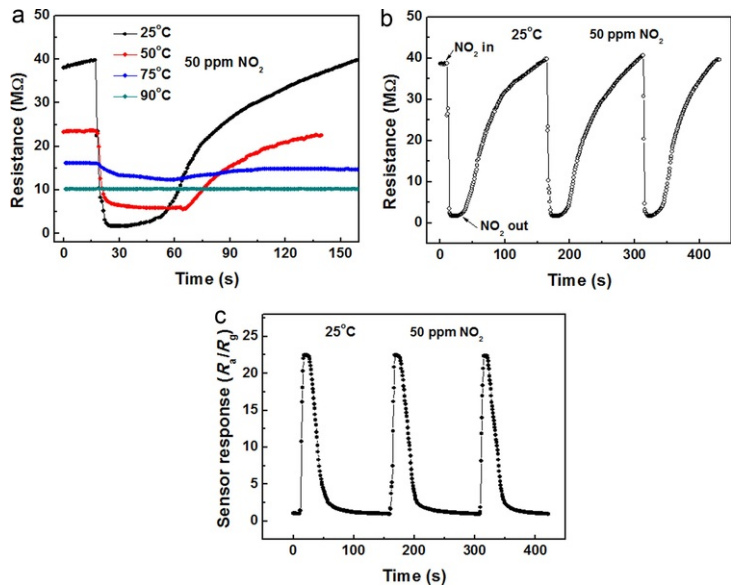
Fig. 7 (a) The real-time resistance changes of Pb(NO$_3$)$_2$-treated PbSe CQDs sensor to 50 ppm NO$_2$ gas at different temperatures, (b) repetitive cycles of resistance variation and (c) corresponding response curve of the Pb(NO$_3$)$_2$-treated PbSe CQDs sensor to 50 ppm NO$_2$ gas at 25 °C.

alt-text: Fig. 7

Table 1 Comparison of the sensing properties of our PbSe CQDs sensor and the other NO$_2$ sensors based on metal sulfide or selenide semiconductors reported in literatures.

alt-text: Table 1

Materials	T (°C)	NO$_2$ (ppm)	Response	t$_{res}$/t$_{rec}$ (s)	Ref.
PbSe CQD	25	50	22.3	7/39	This work
PbS film	38	100	~1.74	20/>1000	[38]
CdS film	38	100	~1.61	50/720	[39]
SnS crystals	25	1	~1.6	–	[35]
SnS$_2$ flakes	120	10	~36	~170/~140	[40]
ZnSe nanowire	25	5	3.34	~80/~40	[29]
ZnS nanowire	300	5	~2.63	72/68	[41]

Fig. 8a further exhibited the response performance of the PbSe sensor to different NO$_2$ concentrations of 100, 70, 50, 30, 20, 10, 5, 10, 20, 30, 50, 70 and 100 ppm in sequences. Evidently, the response sensitivity firstly showed a step-wise decrease with decreasing NO$_2$ concentrations, followed by an increase with further increase in the NO$_2$ concentrations. The sensor response, response and recovery times of the forward and backward cycles were compared and shown in Fig. 8b–d. Results showed a good repeatability when the sensor was tested at different NO$_2$ concentrations. Due to its nonlinear nature of the curve, the calibration curves and the experimental data of the response values could be fitted and the results were listed as follows:

$$\beta_{\text{Forward}} = -14.48 * \exp\left(-C_{\text{Forward}}/24.77\right) + 25.67 \qquad (2)$$

$$\beta_{\text{Backward}} = -13.30 * \exp\left(-C_{\text{Backward}}/27.92\right) + 24.37 \qquad (3)$$

where β is the sensor response and C is the concentration of the NO$_2$ gas. The correlative coefficient R^2 was 0.99259 and 0.99214 for the forward and backward cycles, respectively, indicating the excellent exponential relationship. The results can be applied in the quantitative measurements of NO$_2$ concentration.
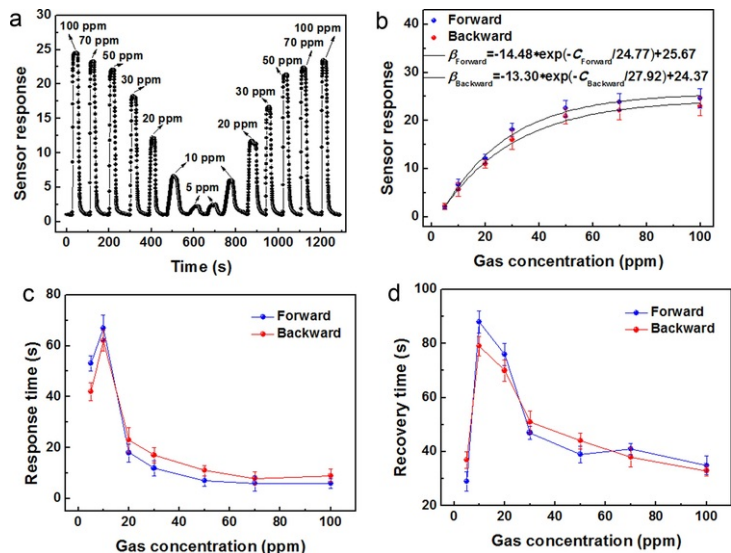

Fig. 8 (a) Gas response curve of PbSe CQDs sensor to different NO$_2$ concentrations. (b)-(d) comparison of the sensor response, response and recovery times of the forward and backward cycles.

alt-text: Fig. 8

Selectivity histogram for the PbSe CQDs sensor was investigated by exposing the gas sensors to different types of gases with a fixed concentration of 50 ppm, including nitrogen dioxide, sulfur dioxide, hydrogen, hydrogen sulfide and ammonia. The results were shown in Fig. 9. Obviously, the sensor showed superior selectivity to NO$_2$ against other interference gases.
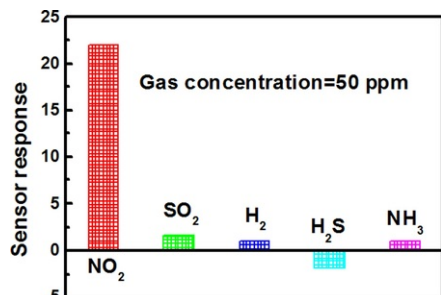

Fig. 9 Selectivity of the PbSe CQDs gas sensor.

alt-text: Fig. 9

3.4 Long-term and humidity stability of the PbSe CQDs sensor

To evaluate the long-term stability of the sensor in atmospheric conditions, we conducted the stability measurement of PbSe CQDs sensor performed over a period of 20 days under laboratory conditions (50 ± 10 RH%, 25 ± 1 °C). The sensor were relatively stable with a variation of about 14.8% of the sensor response after repeated exposure to 50 ppm of NO$_2$ gas for 20 days (Fig. 10a), which might due to the air-stability of the PbSe CQDs itself. Then we further verified the stability of PbSe CQDs solutions and Pb(NO$_3$)$_2$-treated PbSe CQDs films by tracking the position of the first exciton absorption peak over time. As shown in Fig. 10b, the PbSe CQDs synthesized via cation exchange were quite stable in air when stored in octane for 20 days, as its position of the absorption peak and the full width at half maximum (FWHM) were well remained. This was attributed to the chloride passivation and thus

prevent oxidation [31]. However, for the Pb(NO$_3$)$_2$-treated PbSe CQDs film, a 10-nm blue shift of the absorption peak was observed after 20 days. We speculated that the blue shift resulted from the surface etching when the PbSe film was exposed to air for a long time, while it did not lead to great changes in the sensor response. The gas sensing performance of the sensor to 50 ppm NO$_2$ at different humidity conditions were further measured in Fig. 10c. The relative humidity (RH) values were controlled by filling a N$_2$ gas flow passing through saturated aqueous solutions of different salts of CH$_3$COOK, Mg(NO$_3$)$_2$, NaNO$_3$, and KNO$_3$ at 25 °C, which yielded 22%, 54%, 74% and 93% RH, respectively. Fig. 10d showed the effect of relative humidity on the NO$_2$ response and response time. The gas response decreased while response time increased as the increasing relative humidity. This observation may be explained that at a high relative humidity, water molecules adsorbed on the surface of PbSe CQDs, occupying the active sites and blocking off the apertures [42,43]. As a result, the adsorption and diffusion of NO$_2$ molecule were interfered, resulting in lower and slower sensor response.
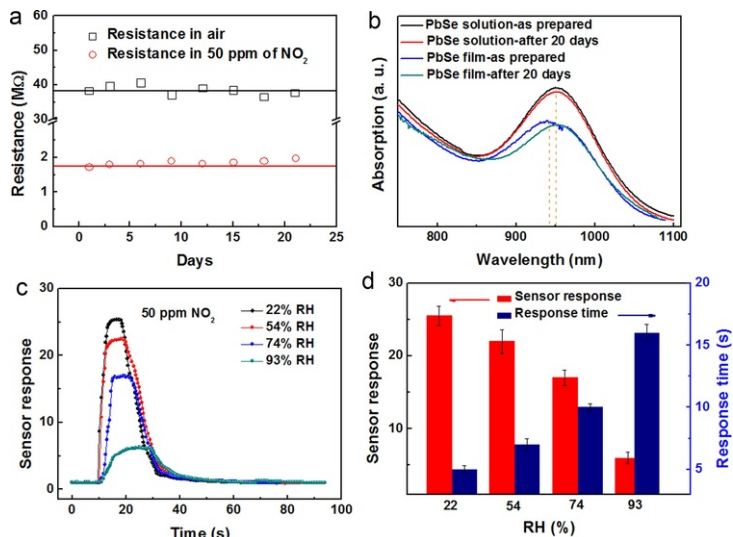

Fig. 10 (a) Long-term stability of the PbSe CQDs gas sensor. (b) Absorption spectra of the as-prepared PbSe CQDs solution and Pb(NO$_3$)$_2$-treated PbSe CQDs film, and those placed in air for 20 days. (c) Response curves of the PbSe CQDs sensor to 50 ppm NO$_2$ at different relative humidity at 25 °C. (d) Gas response and response time as a function of the relative humidity.

alt-text: Fig. 10

3.5 Sensing mechanism

To understand the mechanism underlying the NO$_2$-sensing properties of the PbSe CQDs gas sensor, we first conducted Hall effect experiment to determine the type of the Pb(NO$_3$)$_2$-treated PbSe CQDs film. Table 2 showed the obtained Hall measurement values. The positive sign of Hall coefficient confirmed that our PbSe CQDs film was a p-type semiconductor with holes as majority carriers, which was in accordance with the literatures [44,45].

Table 2 Hall effect measurement values for the Pb(NO$_3$)$_2$-treated PbSe CQDs film.

alt-text: Table 2

PbSe CQD	Resistivity (Ω cm)	Carrier concentration (cm^{-3})	Mobility (cm^{2}V^{-1} s^{-1})
	8×10^{11}	$+4 \times 10^{19}$	2×10^{-3}

Then, in order to understand the interaction of the p-type PbSe film and NO$_2$ gas molecules, we compared XRD and XPS data of the samples before and after NO$_2$ soaking (in 100 ppm NO$_2$ for 12 h to make a more harsh condition). As shown in Fig. 11, neither the XRD pattern nor XPS spectra exhibited detectable variation after NO$_2$ soaking. The peaks in XRD patterns were accorded with cubic PbSe (JCPDS No. 06-0354); the corresponding binding energies of Pb 4f and Se 3d peaks were in accordance with pure PbSe. The results suggested that PbSe CQDs were hard to be oxidized in the presence of NO$_2$ at room temperature. Thus, we speculated that the involved sensing mechanism might not originate from the direct chemical reaction between NO$_2$ and PbSe, but the charge transfer generated by electron extraction from PbSe grains [46].
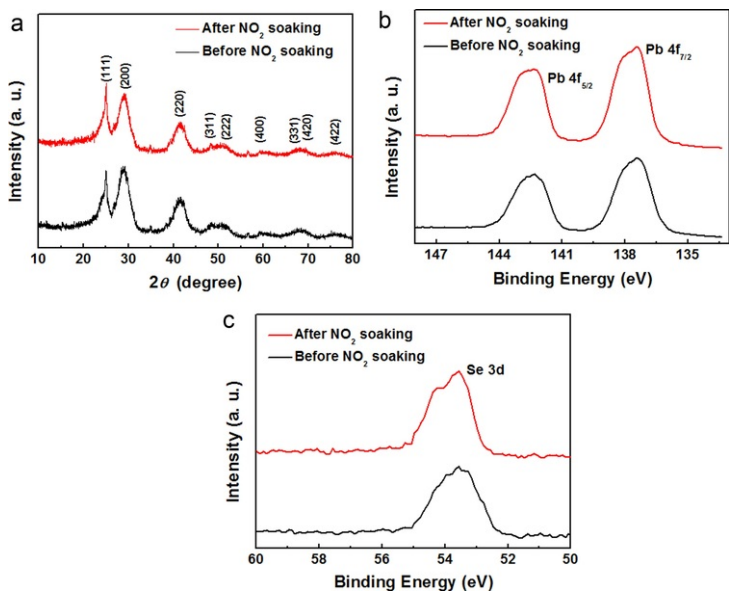
Fig. 11 (a) XRD patterns, (b) Pb 4f core-level XPS spectra and (c) Se 3d core-level XPS spectra of the Pb(NO$_3$)$_2$-treated PbSe CQDs films before and after NO$_2$ soaking (100 ppm, 12 h).

alt-text: Fig. 11

Impedance spectroscopy is a powerful technique to provide insight information about interaction between sensor surface and target gases. The impedance spectra of Pb(NO$_3$)$_2$-treated PbSe CQDs sensor before and after exposure of 100 ppm NO$_2$ at room temperature were shown in Fig. 12a. The obtained experimental data were analyzed by using the equivalent circuit presented in the inset of Fig. 12a, which contained a frequency independent resistance R_0 and a pair RC networks (R_1-bulk resistance, C_1-bulk capacitance, R_2-grain boundary resistance, C_2-grain boundary capacitance). Values of various parameters obtained from impedance spectra were given in Table 3. On exposure to 100 ppm NO$_2$ gas, R_1 and R_2 decreased while C_1 and C_2 increased, which mainly attributed to the reduction in the depth of depletion layer and height of potential barrier at grain boundaries after exposure of NO$_2$ [47,48]. PbSe grains contained considerable fraction of adsorbed oxygen at grain boundaries which trapped electrons from the grains of PbSe and resulted in the forming of barrier to electron transport. On the interaction of PbS film with NO$_2$ gas, adsorbed oxygen on the grain boundary of the PbSe film could be easily kicked out by NO$_2$ gas due to the electron withdrawing nature and higher electron affinity than oxygen [46,49]. The coming NO$_2$ gas trapped electrons from p-type PbSe sensor and led to an increase in charge carrier density (holes), consequently, decreasing the sensor resistance.
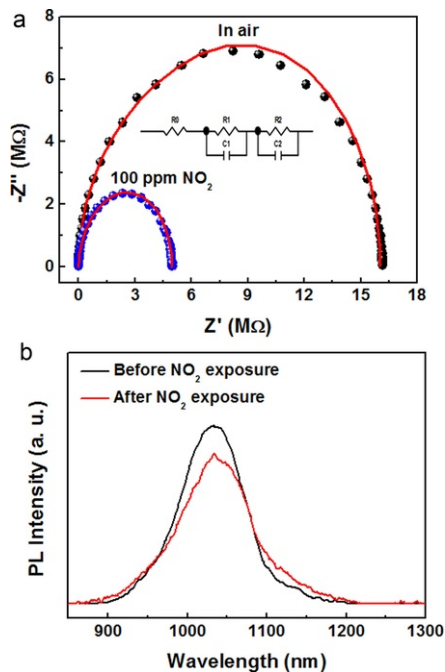
Fig. 12 (a) Impedance spectra of Pb(NO$_3$)$_2$-treated PbSe CQDs sensor before and after exposure to 100 ppm NO$_2$ (The scattered points represented the obtained experimental data and the solid red lines represented the fitting data). Inset showed the equivalent circuit used to interpret the impedance spectroscopy data. (b) PL spectra of Pb(NO$_3$)$_2$-treated PbSe CQDs film before and after exposure to 100 ppm NO$_2$. (For interpretation of the references to colour in this figure legend, the reader is referred to the web version of this article.)

alt-text: Fig. 12

Table 3 Parameters calculated from equivalent circuit to fit the impendence spectra.

alt-text: Table 3

	R_0 (kΩ)	R_1 (MΩ)	C_1 (μF)	R_2 (MΩ)	C_2 (μF)
Unexposed	1	2.8	22	12.2	13
Exposed to 100 ppm NO$_2$	1	1.5	44	0.4	21

Next, we turned our attention to the characterization of PL to study the charge transfer between NO$_2$ and PbSe in depth. Fig. 12b showed the PL spectra of Pb(NO$_3$)$_2$-treated PbSe CQDs film before and after NO$_2$ exposure. A clear emission spectra peaking at approximately 1030 nm was observed, with a 80 nm Stokes shift with respect to the absorption exciton band position. After the NO$_2$ gas molecules were adsorbed, the peak in the PL spectra reduced in intensity, which could be explained by the change of the concentrations of charge carriers [50]. The NO$_2$ molecules on the surface of the PbSe act as electron acceptors and excessive holes were generated by electron extraction from PbSe, introducing more charge-transfer-driven p-type doping. The reduced PL intensity after NO$_2$ exposure might due to the suppression of exciton PL by the injection of excess holes [51]. The results clarified the mechanisms of charge transfer between PbSe and NO$_2$ molecules.

Taking together the above experimental observations, we tried to depicted the energy band diagrams of PbSe CQDs sensor before NO$_2$ injection (air atmosphere), during NO$_2$ injection (NO$_2$ atmosphere) and after NO$_2$ exhausted (air atmosphere) in Fig. 13, and these have been used to discuss the gas-sensing mechanism and kinetics process of gas adsorption and desorption of the PbSe CQDs sensor in detail. In the initial stage before exposed to NO$_2$, oxygen molecules from air adhered to the PbSe CQDs surface and captured electrons, forming oxygen species in the O$_2^-$ form at room temperature [52,53] and an acceptor-like surface state. This created surface state allowed the electrons to be excited from the valence band and induced more holes in the p-type PbSe CQDs, thus forming of an electron-depleted layer near the surface. When exposed to NO$_2$ atmosphere, an oxidizing gas acted as electron

acceptors, the reactions at the PbSe surface can be described using the following reactions:
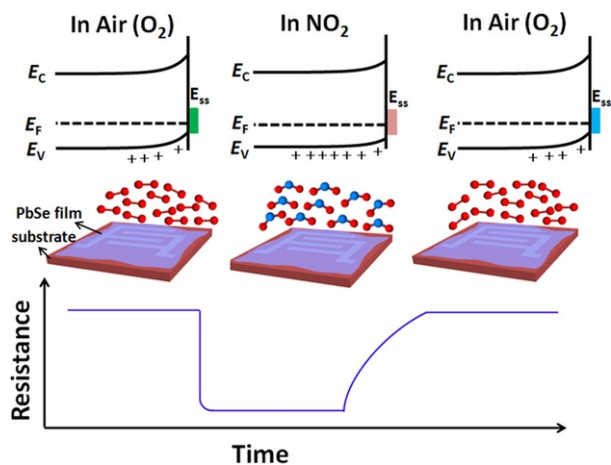
$$NO_{2(gas)} \leftrightarrow NO_{2(ads)} \tag{4}$$

$$NO_{2(ads)} + e^- \leftrightarrow NO_2^- \tag{5}$$

Fig. 13 Schematic diagrams on the gas sensing mechanism of PbSe CQDs based gas sensor and corresponding energy band diagrams (E_{ss} represents surface states).

alt-text: Fig. 13

NO_2 molecules were directly adsorbed on the surface active sites and took electrons away from the PbSe surface. The orbital mixing and hybridization should account for the charge transfer between NO_2 and PbSe [46]. The reaction consumed electrons and increased the hole concentration. Therefore, the depth of electron-depleted layer and height of potential barrier was reduced and accordingly the sensor resistance decreased, because of the oxidizing nature of NO_2 and much higher electron affinity than oxygen. When the NO_2 gas was released and dry air was supplied again, the sensor resistance recovered to its original value. This might be explained that the binding energy of NO_2 on PbSe CQDs surfaces was just moderately higher than oxygen [15], and thus it could be desorbed easily after pumping, leaving behind the captured electrons in the p-type PbSe and decreasing the hole density by electron–hole compensation. Eventually, an increase in resistance was observed. The porous and thin PbSe CQDs film also facilitates the fast gas diffusion and charge transfer, and hence in favor of the rapid response and recovery.

4 Conclusions

In summary, small-size, high-quality and air-stable PbSe colloidal quantum dots were synthesized using a cation exchange method that converts CdSe CQDs directly into PbSe CQDs with in situ chloride and cadmium passivation. The product exhibited near-spherical shape with an extremely small size of 2.87 nm. Gas sensors based on PbSe CQDs were successfully fabricated through spin-coating at room temperature followed with $Pb(NO_3)_2$ treatment. The $Pb(NO_3)_2$-treated PbSe film exhibited p-type semiconductor characteristic and porous surface morphology which facilitated gas adsorption. The PbSe CQDs sensor showed high sensitivity, fast response, full reversibility and superior selectivity to NO_2 gas at room temperature. Moreover, the sensor performance was relatively stable for repeated testing of 20 days under atmospheric pressure with a relative humidity of (50 ± 10)%. The reliable detection of NO_2 make PbSe CQDs attractive candidate for fabrication of low-cost and high-performance NO_2 sensors working at room temperature.

References

[1] N. Barsan, D. Koziej and U. Weimar, Metal oxide-based gas sensor research: how to?, *Sens. Actuators B-Chem.* **121**, 2007, 18–35.

[2] M.E. Franke, T.J. Koplin and U. Simon, Metal and metal oxide nanoparticles in chemiresistors: does the nanoscale matter, *Small* **2**, 2006, 36–50.

[3] L.C. Jia and W.P. Cai, Micro/nanostructured ordered porous films and their structurally induced control of the gas sensing performances, *Adv. Funct. Mater.* **20**, 2010, 3765–3773.

[4] X. Pan, X. Liu, A. Bermak and Z. Fan, Self-gating effect induced large performance improvement of ZnO nanocomb gas sensors, *ACS Nano* **7**, 2013, 9318–9324.

[5] L. Wang, R. Zhang, T.T. Zhou, Z. Lou, J.N. Deng and T. Zhang, Concave Cu_2O octahedral nanoparticles as an advanced sensing material for benzene (C_6H_6) and nitrogen dioxide (NO_2) detection, *Sens. Actuators B-Chem.* **223**, 2016, 311–317.

[6] Y.G. Sun and H.H. Wang, High-Performance, Flexible hydrogen sensors that use carbon nanotubes decorated with palladium nanoparticles, *Adv. Mater.* **19**, 2007, 2818–2823.

[7] J. Ma, Y.K. Liu, H. Zhang, P. Ai, N.L. Gong, Y.M. Wu and D.P. Yu, Room temperature ppb level H_2S detection of a single Sb-doped SnO_2 nanoribbon device, *Sens. Actuators B-Chem.* **216**, 2015, 72–79.

[8] N. Lu, X.Q. Gao, C. Yang, F. Xiao, J.D. Wang and X.T. Su, Enhanced formic acid gas-sensing property of WO_3 nanorod bundles via hydrothermal method, *Sens. Actuators B-Chem.* **223**, 2016, 743–749.

[9] S.Q. Tian, F. Yang, D.W. Zeng and C.S. Xie, Solution-processed gas sensors based on ZnO nanorods array with an exposed (0001) facet for enhanced gas-sensing properties, *J. Phys. Chem. C* **116**, 2012, 10586–10591.

[10] D. Sil, J. Hines, U. Udeoyo and E. Borguet, Palladium nanoparticle-based surface acoustic wave hydrogen sensor, *ACS Appl. Mater. Interfaces* **7**, 2015, 5709–5714.

[11] N. Han, X.F. Wu, L.Y. Chai, H.D. Liu and Y.F. Chen, Counterintuitive sensing mechanism of ZnO nanoparticle based gas sensors, *Sens. Actuators B-Chem.* **150**, 2010, 230–238.

[12] H.M. Huang, H.Y. Li, X.X. Wang and X. Guo, Detecting low concentration of H_2S gas by $BaTiO_3$ nanoparticle-based sensors, *Sens. Actuators B-Chem.* **238**, 2017, 16–23.

[13] J.Y. Kim, O. Voznyy, D. Zhitomirsky and E.H. Sargent, 25th anniversary article: colloidal quantum dot materials and devices: a quarter-century of advances, *Adv. Mater.* **25**, 2013, 4986–5010.

[14] Y. Son, M. Park, Y. Son, J.S. Lee, J.H. Jang, Y. Kim and J. Cho, Quantum confinement and its related effects on the critical size of GeO_2 nanoparticles anodes for lithium batteries, *Nano Lett.* **14**, 2014, 1005–1010.

[15] H. Liu, M. Li, O. Voznyy, L. Hu, Q. Fu, D.X. Zhou, Z. Xia, E. Sargent and J. Tang, Physically flexible, rapid-response gas sensor based on colloidal quantum dot solids, *Adv. Mater.* **26**, 2014, 2718–2724.

[16] M. Li, D.X. Zhou, J. Zhao, Z.P. Zheng, J.G. He, L. Hu, Z. Xia, J. Tang and H. Liu, Resistive gas sensors based on colloidal quantum dot (CQD) solids for hydrogen sulfide detection, *Sens. Actuators B-Chem.* **217**, 2015, 198–201.

[17] H. Liu, M. Li, G. Shao, W.K. Zhang, W.W. Wang, H.B. Song, H.F. Cao, W.L. Ma and J. Tang, Enhancement of hydrogen sulfide gas sensing of PbS colloidal quantum dots by remote doping through ligand exchange, *Sens. Actuators B-Chem.* **212**, 2015, 434–439.

[18] M. Li, W.K. Zhang, G. Shao, H. Kan, Z.L. Song, S.M. Xu, H.X. Yu, S.L. Jiang, J.T. Luo and H. Liu, Sensitive NO_2 gas sensors employing spray-coated colloidal quantum dots, *Thin Solid Films* **618**, 2016, 271–276.

[19] S.J. Oh, Z.Q. Wang, N.E. Berry, J.H. Choi, T.S. Zhao, E.A. Gaulding, T. Paik, Y.M. Lai, C.B. Murray and C.R. Kagan, Engineering charge injection and charge transport for high performance PbSe nanocrystal thin film devices and circuits, *Nano Lett.* **14**, 2014, 6210–6216.

[20] S.J. Oh, C. Uswachoke, T.S. Zhao, J.H. Choi, B.T. Diroll, C.B. Murray and C.R. Kagan, Selective p- and n-doping of colloidal PbSe nanowires to construct electronic and optoelectronic devices, *ACS Nano* **9**, 2015, 7536–7544.

[21] X.H. Wang, G.I. Koleilat, J. Tang, H. Liu, I.J. Kramer, R. Debnath, L. Brzozowski, D.A.R. Barkhouse, L. Levina and S. Hoogland, Tandem colloidal quantum dot solar cells employing a graded recombination layer, *Nat. Photonics* **5**, 2011, 480–484.

[22] G. Konstantatos and E.H. Sargent, Colloidal quantum dot photodetectors, *Infrared Phys. Technol.* **54**, 2011, 278–282.

[23] J.M. Pietryga, R.D. Schaller, D. Werder, M.H. Stewart, V.I. Klimov and J.A. Hollingsworth, Pushing the band gap envelope: mid-infrared emitting colloidal PbSe quantum dots, *J. Am. Chem. Soc.* **126**, 2004, 11752–11753.

[24] J.Y. Woo, J.H. Ko, J.H. Song, K. Kim, H. Choi, Y.H. Kim, D.C. Lee and S. Jeong, Ultrastable PbSe nanocrystal quantum dots via in situ formation of atomically thin halide adlayers on PbSe (100), *J. Am. Chem. Soc.* **136**, 2014, 8883–8886.

[25] A. Shabaev, A.L. Efros and A.L. Efros, Dark and photo-conductivity in ordered array of nanocrystals, *Nano Lett.* **13**, 2013, 5454–5461.

[26] A.D. Yoffe, Semiconductor quantum dots and related systems: electronic, optical, luminescence and related properties of low dimensional systems, *Adv. Phys.* **50**, 2001, 1–208.

[27] O.V. Vassiltsova, Z.Y. Zhao, M.A. Petrukhina and M.A. Carpenter, Surface-functionalized CdSe quantum dots for the detection of hydrocarbons, *Sens. Actuators B-Chem.* **123**, 2007, 522–529.

[28] Z.Q. Lin, F. Liao, L.L. Zhu, S.K. Lu, M.Q. Sheng, S.N. Gao and M.W. Shao, Visible light enhanced gas sensing of CdSe nanoribbons of ethanol, *CrystEngComm* **16**, 2014, 4231–4235.

[29] S. Park, S. Kim, W.I. Lee, K.K. Kim and C. Lee, Room temperature, ppb-level NO_2 gas sensing of multiple-networked ZnSe nanowire sensors under UV illumination, *Beilstein J. Nanotechnol.* **5**, 2014, 1836-1841.

[30] M. Popescu, F. Sava, A. Lorinczi, G. Socol, I.N. Mihailescu, A. Tomescu and C. Simion, Structure, properties and gas sensing effect of SnSe(2) films prepared by pulsed laser deposition method, *J. Non-Cryst. Solids* **53**, 2007, 1865–1869.

[31] J.B. Zhang, J.B. Gao, C.P. Church, E.M. Miller, J.M. Luther, V.I. Klimov and M.C. Beard, PbSe quantum dot solar cells with more than 6% efficiency fabricated in ambient atmosphere, *Nano Lett.* **14**, 2014, 6010–6015.

[32] Q.Q. Dai, Y.N. Wang, X.B. Li, Y. Zhang, D.J. Pellegrino, M.X. Zhao, B. Zou, J. Seo, Y.D. Wang and W.W. Yu, Size-dependent composition and molar extinction coefficient of PbSe semiconductor nanocrystals, *ACS Nano* **3**, 2009, 1518–1524.

[33] J. Kim, C.Y. Wong and G.D. Scholes, Exciton fine structure and spin relaxation in semiconductor colloidal quantum dots, *Acc. Chem. Res.* **42**, 2009, 1037–1046.

[34] W.W. Yu, L.H. Qu, W.Z. Guo and X.G. Peng, Experimental determination of the extinction coefficient of CdTe, CdSe, and CdS nanocrystals, *Chem. Mater.* **15**, 2003, 2854–2860.

[35] J. Wang, G. Lian, Z.H. Xu, C. Fu, Z.J. Lin, L.Y. Li, Q.L. Wang, D.L. Cui and C.P. Wong, Growth of large-size SnS thin crystals driven by oriented attachment and applications to gas sensors and photodetectors, *ACS Appl. Mater. Interfaces* **8**, 2016, 9545–9551.

[36] W.H. Wang, Y. Geng, Y. Qian, M.R. Ji and X.M. Liu, A novel pathway to PbSe nanowires at room temperature, *Adv. Mater.* **10**, 1998, 1479–1481.

[37] T. Ding, H. Wang, S. Xu and J.J. Zhu, Sonochemical synthesis and characterizations of monodispersed PbSe nanocrystals in polymer solvent, *J. Cryst. Growth* **235**, 2002, 517–522.

[38] S.T. Navale, D.K. Bandgar, M.A. Chougule and V.B. Patil, Facile method of preparation of PbS films for NO_2 detection, *RSC Adv.* **5**, 2015, 6518–6527.

[39] S.T. Navale, A.T. Mane, M.A. Chougule, N.M. Shinde, J.H. Kimb and V.B. Patil, Highly selective and sensitive CdS thin film sensors for detection of NO_2 gas, *RSC Adv.* **4**, 2014, 44547–44554.

[40] J.Z. Ou, W.Y. Ge, B. Carey, T. Daeneke, A. Rotbart, W. Shan, Y.C. Wang, Z.Q. Fu, A.F. Chrimes, W. Wlodarski, S.P. Russo, Y.X. Li and K. Kalantar-zadeh, Physisorption-based charge transfer in two-dimensional SnS_2 for selective and reversible NO_2 gas sensing, *ACS Nano* **9**, 2015, 10313–10323.

[41] S. Park, S. An, H. Ko, S. Lee and C. Lee, Synthesis, structure, and UV-enhanced gas sensing properties of Au-functionalized ZnS nanowires, *Sens. Actuators B-Chem.* **188**, 2013, 1270–1276.

[42] H.L. Tian, H.Q. Fan, M.M. Li and L.T. Ma, Zeolitic imidazolate framework coated ZnO nanorods as molecular sieving to improve selectivity of formaldehyde gas sensor, *ACS Sens.* **1**, 2016, 243–250.

[43] H.L. Tian, H.Q. Fan, G.Z. Dong, L.T. Ma and J.W. Ma, NiO/ZnO p?n heterostructures and their gas sensing properties for reduced operating temperature, *RSC Adv.* **6**, 2016, 109091–109098.

[44] H. Wang, Y.Z. Pei, A.D. LaLonde and G.J. Snyder, Heavily doped p-type PbSe with high thermoelectric performance: an alternative for PbTe, *Adv. Mater.* **23**, 2011, 1366–1370.

[45] W.J. Liang, O. Rabin, A.I. Hochbaum, M. Fardy, M.J. Zhang and P.D. Yang, Thermoelectric properties of p-type PbSe nanowires, *Nano Res.* **2**, 2009, 394–399.

[46] Y.Q. Cai, G. Zhang and Y.W. Zhang, Charge transfer and functionalization of monolayer InSe by physisorption of small molecules for gas sensing, *J. Phys. Chem. C* **121**, 2017, 10182–10193.

[47] S.M. Ingole, S.T. Navale, Y.H. Navale, D.K. Bandgar, F.J. Stadler, R.S. Mane, N.S. Ramgir, S.K. Gupta, D.K. Aswal and V.B. Patil, Nanostructured tin oxide films: physical synthesis, characterization, and gas sensing properties, *J. Colloid Interface Sci.* **493**, 2017, 162–170.

[48] M. Kaur, S.K. Gupta, C.A. Betty, V. Saxena, V.R. Katti, S.C. Gadkari and J.V. Yakhmi, Detection of reducing gases by SnO_2 thin films: an impedance spectroscopy study, *Sens. Actuators B-Chem.* **107**, 2005, 360–365.

[49] P. Li, H.Q. Fan, Y. Cai, M.M. Xu, C.B. Long, M.M. Li, S.H. Lei and X.W. Zou, Phase transformation (cubic to rhombohedral): the effect on the NO_2 sensing performance of Zn-doped flower-like In_2O_3 structures, *RSC Adv.*

4, 2014, 15161–15170.

[50] B. Cho, M.G. Hahm, M. Choi, J. Yoon, A.R. Kim, Y.J. Lee, S.G. Park, J.D. Kwon, C.S. Kim, M. Song, Y. Jeong, K.S. Nam, S. Lee, T.J. Yoo, C.G. Kang, B.H. Lee, H.C. Ko, P.M. Ajayan and D.H. Kim, Charge-transfer-based gas sensing using atomic-layer MoS$_2$, *Sci. Rep.* **5**, 2015, 8052.

[51] S. Mouri, Y. Miyauchi and K. Matsuda, Tunable photoluminescence of monolayer MoS$_2$ via chemical doping, *Nano Lett.* **13**, 2013, 5944–5948.

[52] J. Zhang, X.H. Liu, G. Neri and N. Pinna, Nanostructured materials for room-temperature gas sensors, *Adv. Mater.* **28**, 2016, 795–831.

[53] X.W. Zou, H.Q. Fan, Y.M. Tian, M.G. Zhang and X.Y. Yan, Microwave-assisted hydrothermal synthesis of Cu/Cu$_2$O hollow spheres with enhanced photocatalytic and gas sensing activities at room temperature, *Dalton Trans.* **44**, 2015, 7811–7821.

Min Li received her doctoral degree in School of Optical and Electronic Information from Huazhong University of Science and Technology, China in 2016. She is currently a postdoctor in Shenzhen Key Laboratory of Advanced Thin Films and Applications, college of Physics and Energy, Shenzhen University, China. Her research focuses on colloidal quantum dots and thin film gas sensors.

Jingting Luo received the Ph.D. degree from Tsinghua University, Beijing, China, in 2012. From January 2016, he has been working as an academic visitor in Faculty of Engineering and Environment, University of Northumbria at Newcastle, UK. He is currently an associate professor in College of Physics and Energy of Shenzhen University, Shenzhen, China.

Chen Fu received his Bachelor's degree from Chinese University of Geoscience, Beijing (CUGB) in 2005. In 2011, He received his Ph.D. degree from the Institute of Acoustics (IOA), Chinese Academy of Sciences. Since 2011, he worked as a postdoctoral researcher at Ajou University in South Korea and then at Newcastle university in UK. He now works as an assistant professor at Shenzhen University. His current research interest is on SAW theory and the application of SAW sensors.

Hao Kan received his Master's degree in College of Optoelectronic Engineering from Shenzhen University, China in 2013. He is currently a PhD degree candidate in School of Optical and Electronic Information at Huazhong University of Science and Technology, China. His research focuses on gas sensors and photodetectors.

Zhen Huang received his Master's degree in School of Optical and Electronic Information at Huazhong University of Science and Technology, China in 2016. He is currently a PhD degree candidate in School of Optical and Electronic Information at Huazhong University of Science and Technology, China. His research focuses on CQD photovoltaics.

Wangman Huang received his Bachelor's degree in School of Optical and Electronic Information at Huazhong University of Science and Technology, China in 2016. He is currently a Master degree candidate in School of Optical and Electronic Information at Huazhong University of Science and Technology, China. His research focuses on surface acoustic wave (SAW) gas sensors.

Shuqin Yang received her Bachelor's degree in Faculty of Physics and Electronic Technology at Hubei University, China in 2016. She is currently a Master degree candidate in School of Optical and Electronic Information at Huazhong University of Science and Technology, China. Her research focuses on CQD gas sensors.

Jianbing Zhang has been an associate professor of School of Optical and Electronic Information at Huazhong University of Science and Technology, China since 2010. He received his Master's degree and PhD degree in micro- and solid-state electronics from Huazhong University of Science and Technology in 2006 and 2010 respectively. From 2012 to 2014, he had been a post-doctoral fellow at National Renewable Energy Laboratory, USA. His research interests include micro/nano semiconductor materials and solar cell materials and devices.

Jiang Tang is a full professor at Wuhan National Laboratory for Optoelectronics (WNLO), Huazhong University of Science and Technology. He obtained his Bachelor's degree from University of Science and Technology of China, and his PhD from University of Toronto under the supervision of Prof. Edward H. Sargent. After graduation, he moved to IBM T. J. Watson research center working on copper zinc tin sulfide solar cells as a postdoctoral researcher. Based on his intensive research experience in PbS colloidal quantum dot (CQDs) solar cells and photodetectors, he started working on PbS CQDs gas sensors at WNLO, as well as thin film photovoltaics.

Honglang Li received his B.S. degree in microelectronics from Hunan University in 1998 and Ph.D. degree in acoustics from the Institute of Acoustics, Chinese Academy of Sciences, in 2003. From 2003 to 2005, he joined the Venture Business Laboratory, Chiba University, as a post-doctoral fellow, and is now an research fellow in the Institute of Acoustics, Chinese Academy of Sciences from 2011. His current research is on optimization of surface acoustic wave devices, acoustic sensors, and their application in RFIC.

Huan Liu has been an associate professor of School of Optical and Electronic Information at Huazhong University of Science and Technology, China since 2011. She received her Master's degree and PhD degree in micro- and solid-state electronics from Huazhong University of Science and Technology in 2004 and 2008 respectively. From 2009 to 2011, she had been a post-doctoral fellow in the Department of Electrical and Computer Engineering at University of Toronto, Canada. Her research interests include nanostructured functional materials, gas sensors and photovoltaics.

Highlights

- Small-size, high-quality and air-stable PbSe CQDs were synthesized by a cation exchange method in solution.

- Room temperature NO_2 gas sensors based on PbSe CQDs have been demonstrated.

- The long-term stability of the sensor was certified.

Queries and Answers

Query: The author names have been tagged as given names and surnames (surnames are highlighted in teal color). Please confirm if they have been identified correctly.
Answer: Yes

Query: "Your article is registered as a regular item and is being processed for inclusion in a regular issue of the journal. If this is NOT correct and your article belongs to a Special Issue/Collection please contact s.sandacoumar@elsevier.com immediately prior to returning your corrections."
Answer: Yes, the article belongs to a regular issue.

Query: One or more sponsor names and the sponsor country identifier may have been edited to a standard format that enables better searching and identification of your article. Please check and correct if necessary.
Answer: Yes

Query: Fig. 12 will appear in black and white in print and in color on the web. Based on this, the respective figure caption has been updated. Please check, and correct if necessary.
Answer: Yes, we have checked it.